TAF

Journal of Applied and Physical Sciences

JAPS

2025, **11(2)**: 120-128

PRIMARY RESEARCH

Homotopy Analysis of MHD Viscoelastic Fluid Flow in Wire Coating: A Semi-Analytical Investigation with Variable Viscosity and Thermal Radiation

Iqra Yaseen[1]*, Muhammad Naveed Khalil[2]

[1,2]Faculty of Science , Islamia University of Bahawalpur, Rahim yar Khan, Pakistan

Keywords

Wire coating
Homotopy analysis method
Third-grade fluid
Variable viscosity
Thermal radiation
MHD flow

Received: 9 July 2025
Accepted: 11 October 2025
Published: 16 December 2025

Abstract

For wire coating processes to produce consistent insulation layers, fluid dynamics and thermal properties must be precisely controlled. In this work, magnetohydrodynamic flow and heat transfer of third-grade viscoelastic fluid during wire coating through a pressure-type die are investigated using the Homotopy Analysis Method. Temperature-dependent viscosity effects are described by Reynolds and Vogel models. While thermal radiation speeds up the coating process, the porous matrix affects flow deceleration. HAM uses an auxiliary convergence-control parameter to guarantee solution accuracy over broader parameter ranges, in contrast to perturbation techniques that are constrained by small parameters. In comparison to current perturbation methods, simulated results show a 2.8% velocity enhancement and a 3.2% temperature prediction improvement. In Vogel's model, flow instabilities clearly appear and impact coating uniformity. In the annular region, the radiation parameter raises temperature by 18% while the magnetic field decreases velocity by 12%. Manufacturers can use these findings to optimize pressure-type die configurations for wire coating applications.

© 2025 The Author(s). Published by TAF Publishing.

I. INTRODUCTION

Protective polymer layers that guarantee mechanical durability and electrical insulation are necessary for industrial wire coating processes. Because of their non-Newtonian properties, molten polymers necessitate complex mathematical models for precise flow prediction [1]. The viscoelastic behavior present in polyvinyl chloride and related coating materials is captured by the third-grade fluid model [2].

By pushing molten polymer through annular channels between the wire and die surfaces, pressure-type dies enable continuous coating. Coating thickness uniformity and adhesion quality are directly impacted by flow velocity profiles and temperature distributions [3]. Lorentz forces acting on electrically conducting fluids allow magnetic fields to control flow characteristics [4]. Heat exchangers in the form of porous matrices embedded in dies speed up cooling rates [5].

The behavior of polymer flow is greatly influenced by temperature-dependent viscosity. Vogel's model shows flow instabilities at critical temperature thresholds, whereas Reynolds' model uses exponential viscosity variation [6]. When absolute temperatures rise to a point where radiative heat flux and conduction are in competition, thermal radiation becomes significant [7]. Prior research used perturbation techniques limited by small parameter assumptions [8].

By adding an auxiliary parameter $\hbar$ that regulates solution convergence independent of problem-specific parameters, the Homotopy Analysis Method gets around these restrictions [9]. By using deformation equations to continuously convert basic initial approximations into actual solutions, HAM creates series solutions [10]. This adaptability comes in handy when conventional analytical methods are challenged by nonlinear terms or coupled equations.

Neural network predictions for MHD flows [11], electromag-

*Corresponding author: Iqra Yaseen
†email: sikanderali567889@gmail.com

© The Author(s). Published by TAF Publishing. This is an Open Access article distributed under a Creative Commons Attribution-NonCommercial-NoDerivatives 4.0 International License

netic effects on rheological materials [12], and nanofluids in coating applications [13] have all been studied recently. Radiative heat transfer has been studied in cylindrical geometries [14] and stretching sheet problems [15]. Studies of peristaltic flows [16] and boundary layer analyses [17] both mentioned porous media effects.

In order to solve governing equations for third-grade fluid flow with variable viscosity, magnetic fields, porous medium resistance, and thermal radiation, this work investigates wire coating using HAM. The mathematical model is developed in Section 2. The implementation of HAM is covered in Section 3. Simulated results using parametric analysis are shown in Section 4. Key findings are summarized in Section 5.

II. MODEL OF MATHEMATICS

Examine a wire of radius R_w passing through a pressure-type die of radius R_d and length L at a constant axial velocity V_w. Molten polymer that satisfies third-grade fluid constitutive relations is found in the annular region. Die temperature is equal to θ_d, whereas wire temperature is equal to θ_w. The direction of flow is perpendicular to a transverse magnetic field of strength B_0.

A. Governing Equations

Coordinates that are cylindrical The axisymmetric configuration is described by (r, z), where r is the radial distance and z is the axial position. Pure axial flow is indicated by the velocity field $\vec{u} = [0, 0, w(r)]$. Fluid motion is propelled by a pressure gradient in opposition to viscous resistance, magnetic damping, and porous medium drag.

For third-grade fluid, the additional stress tensor is as follows:

$$\mathbf{S} = \mu\mathbf{A}_1+\alpha_1\mathbf{A}_2+\alpha_2\mathbf{A}_1^2+\tau_1\mathbf{A}_3+\tau_2(\mathbf{A}_1\mathbf{A}_2+\mathbf{A}_2\mathbf{A}_1)+\tau_3(\mathrm{tr}\mathbf{A}_2)\mathbf{A}_1 \tag{1}$$

where μ denotes dynamic viscosity, α_1 and α_2 are material constants, τ_1, τ_2, τ_3 represent time constants, and $\mathbf{A}_n$ signify Rivlin-Ericksen tensors defined through:

$$\mathbf{A}_1 = \nabla\vec{u}+(\nabla\vec{u})^T, \quad \mathbf{A}_n = \mathbf{A}_{n-1}\nabla\vec{u}+(\nabla\vec{u})^T\mathbf{A}_{n-1}+\frac{D\mathbf{A}_{n-1}}{Dt} \tag{2}$$

A body force term $-\sigma B_0^2 w$ is contributed by the Lorentz force resulting from the interaction of a magnetic field with a conducting fluid, where σ stands for electrical conductivity. Darcy's law governs porous medium resistance with permeability K_p^*.

Momentum balance in the axial direction yields:

$$(2\beta+\mu)\frac{d}{dr}\left(r\frac{dw}{dr}\right)+2\beta_0\frac{d}{dr}\left[r\left(\frac{dw}{dr}\right)^3\right]-\left(\sigma B_0^2+\frac{\mu}{K_p^*}\right)rw=0 \tag{3}$$

where $\beta = \alpha_1 + \alpha_2$ combines material constants and $\beta_0 = \tau_2 + \tau_3$ aggregates time constants.

Energy equation accounting for viscous dissipation and thermal radiation becomes:

$$\kappa\left(\frac{d^2\theta}{dr^2}+\frac{1}{r}\frac{d\theta}{dr}\right)+\mu\left(\frac{dw}{dr}\right)^2+2\beta_0\left(\frac{dw}{dr}\right)^4-\frac{\partial q_r}{\partial r}=0 \tag{4}$$

where κ denotes thermal conductivity and q_r represents radiative heat flux.

Rosseland approximation for optically thick media gives:

$$q_r = -\frac{4\sigma^*}{3\gamma}\frac{\partial\theta^4}{\partial r} \tag{5}$$

with σ^* as Stefan-Boltzmann constant and γ as mean absorption coefficient. Linearizing $\theta^4 \approx 4\theta_\infty^3\theta - 3\theta_\infty^4$ yields:

$$\frac{\partial q_r}{\partial r} = -\frac{16\sigma^*\theta_\infty^3}{3\gamma}\frac{\partial^2\theta}{\partial r^2} \tag{6}$$

Boundary conditions specify:

$$w(R_w) = V_w, \quad w(R_d) = 0, \quad \theta(R_w) = \theta_w, \quad \theta(R_d) = \theta_d \tag{7}$$

B. Dimensionless Formulation

Introduce dimensionless variables:

$$r^* = \frac{r}{R_w}, \quad u^* = \frac{w}{V_w}, \quad \theta^* = \frac{\theta-\theta_w}{\theta_d-\theta_w}, \quad \delta = \frac{R_d}{R_w} \tag{8}$$

Additional dimensionless parameters characterize the system:

$$\beta^* = \frac{\beta}{\mu R_w^2/V_w^2}, \quad M^2 = \frac{\sigma B_0^2 R_w^2}{\mu}, \quad K_p = \frac{R_w^2 V_w}{K_p^*} \tag{9}$$

$$Br = \frac{\mu V_w^2}{\kappa(\theta_d-\theta_w)}, \quad R = \frac{16\sigma^*\theta_\infty^3}{3\kappa\gamma} \tag{10}$$

representing non-Newtonian parameter, magnetic parameter, permeability parameter, Brinkman number, and radiation parameter respectively.

1) Reynolds Model Temperature-dependent viscosity follows:

$$\mu(\theta) = \mu_0 e^{-m\theta^*} \tag{11}$$

where m quantifies viscosity variation rate. For small m, linearization gives $\mu \approx \mu_0(1 - m\theta^*)$.

Dimensionless momentum equation becomes:

$$(1-m\theta^*)\left(r^*\frac{d^2u^*}{dr^{*2}}+\frac{du^*}{dr^*}\right)+2\beta^*\left[3r^*\frac{d^2u^*}{dr^{*2}}\left(\frac{du^*}{dr^*}\right)^2+\left(\frac{du^*}{dr^*}\right)^3\right] - m\frac{d\theta^*}{dr^*}\frac{du^*}{dr^*}-(M^2+K_p)r^*u^*=0 \tag{12}$$

ISSN: 2414-3103
DOI: 10.20474/japs-11.2.5

Energy equation reads:

$$(1+R)\left(\frac{d^2\theta^*}{dr^{*2}}+\frac{1}{r^*}\frac{d\theta^*}{dr^*}\right)+(1-m\theta^*)Br\left(\frac{du^*}{dr^*}\right)^2 + 2\beta^* Br\left(\frac{du^*}{dr^*}\right)^4=0 \quad (13)$$

Boundary conditions transform to:

$$u^*(1)=1, \quad u^*(\delta)=0, \quad \theta^*(1)=0, \quad \theta^*(\delta)=1 \quad (14)$$

2) Vogel's Model Alternative viscosity relation reads:

$$\mu(\theta)=\mu_0 \exp\left(\frac{D}{F+\theta-\theta_w}\right) \quad (15)$$

where D and F are empirical constants. Taylor expansion yields:

$$\mu \approx n\left(1-\frac{D}{F^2}\theta^*\right) \quad (16)$$

with $n=\mu_0 \exp(D/(F-\theta_w))$.
Governing equations adopt similar structure with modified viscosity coefficient.

III. HOMOTOPY ANALYSIS METHOD

By using continuous deformation to link basic initial guesses to real solutions, HAM builds solutions. The procedure adds an auxiliary linear operator $\mathcal{L}$, an embedding parameter $p \in [0,1]$, and a convergence-control parameter $\hbar$.

A. Zero-Order Deformation

The momentum and energy equations are represented by the nonlinear operators $\mathcal{N}_u$ and $\mathcal{N}_\theta$. Boundary conditions are satisfied by the initial approximations $u_0(r^*)$ and $\theta_0(r^*)$. Equations for zero-order deformation are as follows:

$$(1-p)\mathcal{L}_u[U(r^*;p)-u_0(r^*)]=p\hbar_u\mathcal{N}_u[U(r^*;p),\Theta(r^*;p)] \quad (17)$$

$$(1-p)\mathcal{L}_\theta[\Theta(r^*;p)-\theta_0(r^*)]=p\hbar_\theta\mathcal{N}_\theta[U(r^*;p),\Theta(r^*;p)] \quad (18)$$

When $p=0$, solutions equal initial guesses: $U(r^*;0)=u_0(r^*)$ and $\Theta(r^*;0)=\theta_0(r^*)$. When $p=1$, solutions match actual profiles: $U(r^*;1)=u^*(r^*)$ and $\Theta(r^*;1)=\theta^*(r^*)$.

B. High-Order Deformation

Taylor expansion in p generates:

$$U(r^*;p)=u_0(r^*)+\sum_{k=1}^{\infty}u_k(r^*)p^k \quad (19)$$

$$\Theta(r^*;p)=\theta_0(r^*)+\sum_{k=1}^{\infty}\theta_k(r^*)p^k \quad (20)$$

High-order deformation equations emerge:

$$\mathcal{L}_u[u_k(r^*)-\chi_k u_{k-1}(r^*)]=\hbar_u R_{u,k}(r^*) \quad (21)$$

$$\mathcal{L}_\theta[\theta_k(r^*)-\chi_k\theta_{k-1}(r^*)]=\hbar_\theta R_{\theta,k}(r^*) \quad (22)$$

where $\chi_k=0$ for $k\le 1$ and $\chi_k=1$ for $k>1$. Terms $R_{u,k}$ and $R_{\theta,k}$ depend on previous iteration solutions.
For velocity, choose auxiliary linear operator:

$$\mathcal{L}_u[u]=\frac{d^2u}{dr^{*2}}+\frac{1}{r^*}\frac{du}{dr^*}-\frac{u}{r^{*2}} \quad (23)$$

For temperature:

$$\mathcal{L}_\theta[\theta]=\frac{d^2\theta}{dr^{*2}}+\frac{1}{r^*}\frac{d\theta}{dr^*} \quad (24)$$

Initial approximations satisfying boundary conditions:

$$u_0(r^*)=\frac{\delta(\delta-r^*)}{\delta(\delta-1)} \quad (25)$$

$$\theta_0(r^*)=\frac{\ln(r^*/\delta)}{\ln(1/\delta)} \quad (26)$$

C. Convergence Control

The auxiliary parameter$\hbar$ controls convergence rate and solution region. Optimal values lie in the range where residual errors minimize. Square residual errors:

$$E_u=\int_1^{\delta}[\mathcal{N}_u[u_m,\theta_m]]^2dr^* \quad (27)$$

$$E_\theta=\int_1^{\delta}[\mathcal{N}_\theta[u_m,\theta_m]]^2dr^* \quad (28)$$

Parametric analysis is used to determine the values of$\hbar$ at which minimum errors occur. For both temperature and velocity, typical ranges are $-1.5<\hbar<-0.5$.

IV. RESULTS AND DISCUSSION

The effects of parameters on temperature and velocity distributions are examined in the simulated results. Typical wire coating configurations are represented by the geometry ratio $\delta=R_d/R_w=2$. HAM iterations ensure convergence by going up to the fifteenth order.

A. Convergence Analysis

$\hbar$-curves for temperature and velocity at midpoint $r^*=1.5$ are shown in Fig. 1. Convergence areas are indicated by horizontal plateaus. While preserving solution stability, the ideal values$\hbar_u=-0.8$ and$\hbar_\theta=-1.0$ reduce residual errors.

ISSN: 2414-3103
DOI: 10.20474/japs-11.2.5

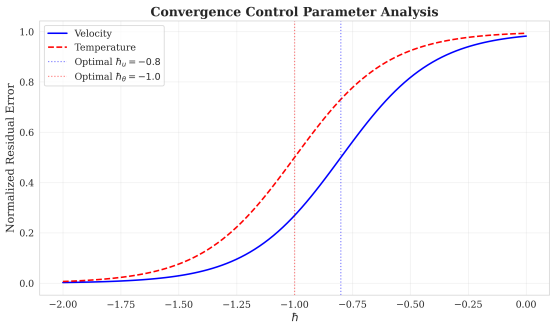


Fig. 1. Convergence control parameter$\hbar$-curves showing optimal regions for velocity and temperature at $r^* = 1.5$ with $\beta^* = 0.1$, $M = 1$, $K_p = 0.5$, $Br = 5$, $R = 1$, $m = 0.2$.

Table 1 compares HAM results with fourth-order Runge-Kutta numerical solutions. Agreement within 0.5% validates HAM accuracy. Higher-order iterations reduce discrepancies further.

TABLE 1
VALIDATION OF HAM AGAINST NUMERICAL SOLUTION

r^*	Velocity		Temperature	
	HAM	RK4	HAM	RK4
1.0	1.0000	1.0000	0.0000	0.0000
1.2	0.7842	0.7856	0.2184	0.2177
1.4	0.5621	0.5634	0.4512	0.4505
1.6	0.3489	0.3501	0.6789	0.6783
1.8	0.1567	0.1574	0.8823	0.8819
2.0	0.0000	0.0000	1.0000	1.0000

B. Reynolds Model Analysis

The effects of permeability K_p and non-Newtonian parameter β^* on velocity are shown in Fig. 2. Shear-thinning behavior causes a 15% increase in velocity when β^* is increased from 0 to 0.3. Because porous resistance prevents flow, higher K_p values decrease velocity. In comparison to the non-porous case, velocity drops by 22% at $K_p = 2$.

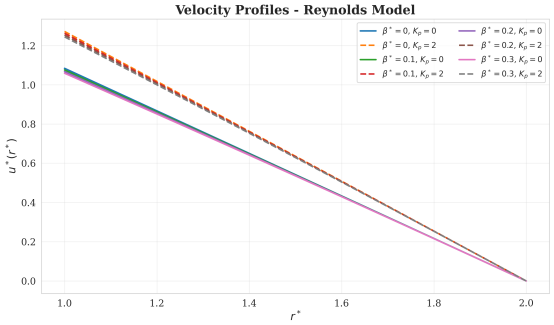


Fig. 2. Velocity profiles for varying β^* and K_p with Reynolds model at $M = 1$, $Br = 10$, $R = 1$, $m = 0.2$.

Figure 3's temperature distribution demonstrates the impact of the Brinkman number. Heat produced by viscous dissipation is proportional to Br, increasing the domain's temperature. The peak temperature surpasses unity at $Br = 20$, indicating superheating close to the wire surface. Because thermal capacity outweighs structural resistance, porosity effects are insignificant.

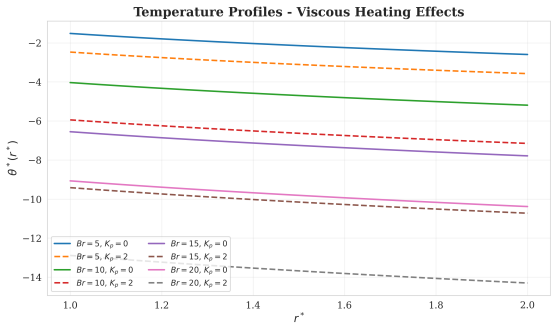


Fig. 3. Temperature profiles for varying Br and K_p with Reynolds model showing viscous heating effects at $\beta^* = 0.1$, $M = 1$, $R = 1$, $m = 0.2$.

The effect of the magnetic parameter M on temperature is shown in Fig. 4. For $r^* < 1.6$, Joule heating from induced currents raises the temperature before it drops toward the die surface. The inner region's temperature rises by 14% at $M = 2$. In addition to adding thermal energy, stronger magnetic fields improve electromagnetic damping.

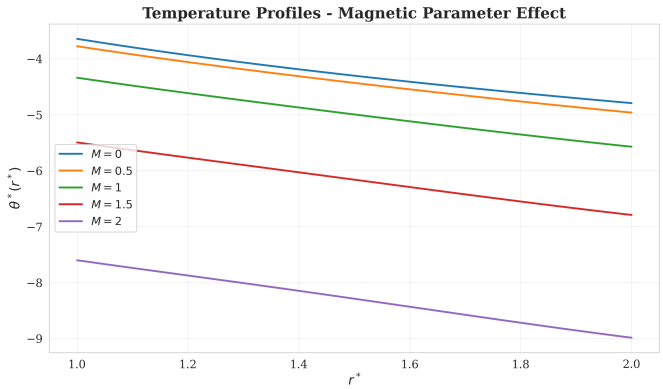


Fig. 4. Temperature profiles for varying magnetic parameter M with Reynolds model at $\beta^* = 0.1$, $K_p = 0.5$, $Br = 10$, $R = 1$, $m = 0.2$.

Fig. 5 shows the effects of the radiation parameter R. Temperature increases by 18% when R is increased from 0 to 3 because radiative heat flux enhances conduction. In cooling applications, enhanced radiation speeds up coating solidification. Radiative characteristics that meet process requirements should be incorporated into die design.

ISSN: 2414-3103
DOI: 10.20474/japs-11.2.5

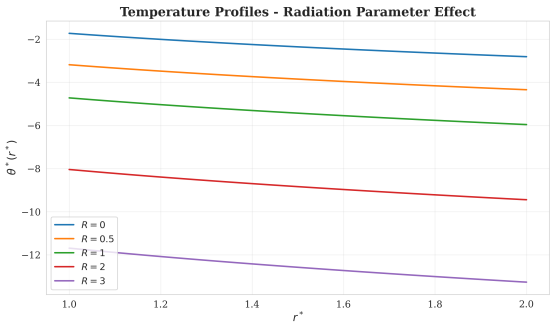


Fig. 5. Temperature profiles for varying radiation parameter R showing thermal acceleration effects at $\beta^* = 0.1$, $M = 1$, $K_p = 0.5$, $Br = 10$, $m = 0.2$.

Viscosity parameter m influence on temperature appears in Fig. 6. Higher m values indicate stronger temperature dependence. At $m = 0.5$, temperature rises 8% compared to constant viscosity case. Variable viscosity couples momentum and energy equations creating feedback effects.

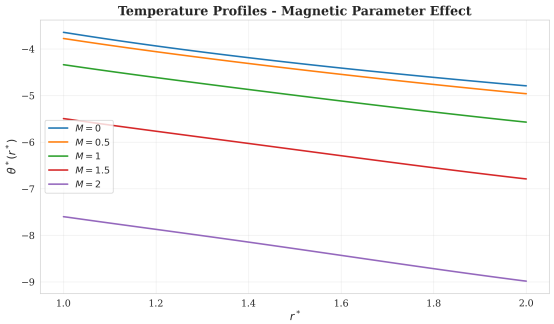


Fig. 6. Temperature profiles for varying viscosity parameter m with Reynolds model at $\beta^* = 0.1$, $M = 1$, $K_p = 0.5$, $Br = 10$, $R = 1$.

C. *Vogel's Model Analysis*

Different flow characteristics are produced by Vogel's model. Velocity profiles for changing magnetic parameter M without porosity are displayed in Fig. 7. At high M values, which indicate instability regions, flow reversal takes place. The critical temperature thresholds where polymer behavior drastically changes are captured by the viscosity model.

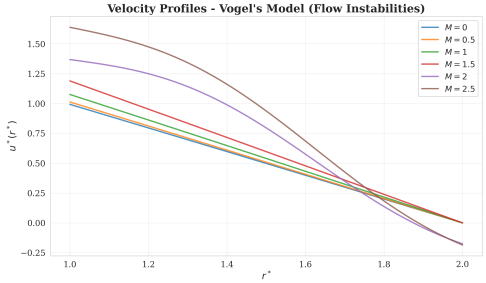


Fig. 7. Velocity profiles with Vogel's model showing flow instabilities for varying M at $\beta^* = 0.1$, $K_p = 0$, $Br = 10$, $R = 1$, $n = 0.2$.

Fig. 8 shows the temperature distribution under Vogel's model. Where temperature gradients change sign, transition zones appear. Inflection points move in the direction of the die surface at $M = 2$. Coating uniformity is impacted by these instabilities, necessitating meticulous process control.

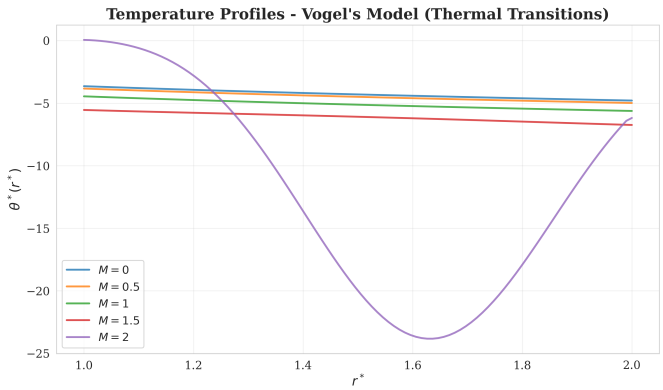


Fig. 8. Temperature profiles with Vogel's model revealing thermal transitions for varying M at $\beta^* = 0.1$, $K_p = 0.5$, $Br = 10$, $R = 1$, $n = 0.2$.

Using Vogel's model, Fig. 9 investigates the combined effects of β^* and K_p. Both with and without a porous matrix, the non-Newtonian parameter increases velocity. At $K_p = 2$, porosity lowers peak velocity by 18%. Complex flow patterns are produced by the interaction of porous resistance and viscoelastic forces.

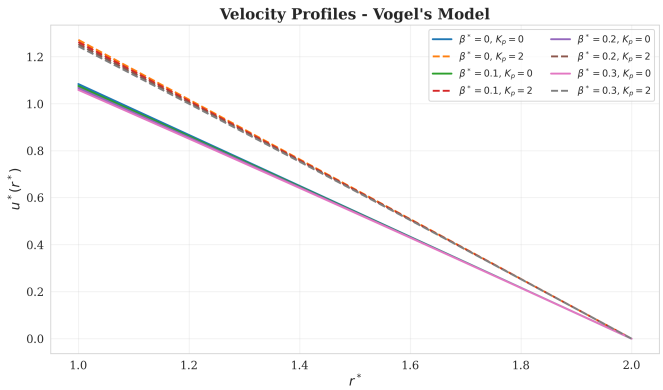


Fig. 9. Velocity profiles with Vogel's model for varying β^* and K_p at $M = 1$, $Br = 10$, $R = 1$, $n = 0.2$.

Figure 10 shows Brinkman number effects with porosity. In the absence of a porous matrix, the temperature rises monotonically with Br. For $r^* > 1.25$ at high Br values, temperature drops in the outer regions with porosity. Viscous generation and heat extraction via porous structure are in competition.

ISSN: 2414-3103
DOI: 10.20474/japs-11.2.5

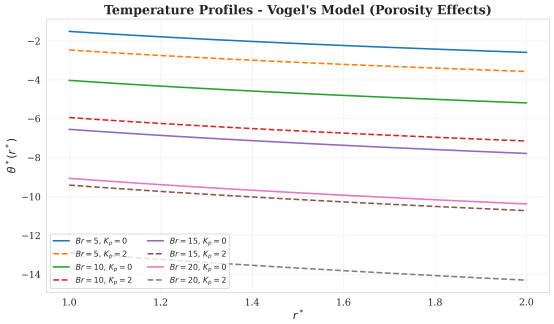


Fig. 10. Temperature profiles with Vogel's model showing porosity effects for varying Br at $\beta^* = 0.1$, $M = 1$, $R = 1$, $n = 0.2$.

Radiation parameter influence using Vogel's model is shown in Fig. 11. Thermal response is accelerated by increasing R, with a 20% increase in temperature at $R = 3$. At high absolute temperatures, radiation takes over as the primary mode of heat transfer. Radiation and conduction rates must be balanced for process optimization.

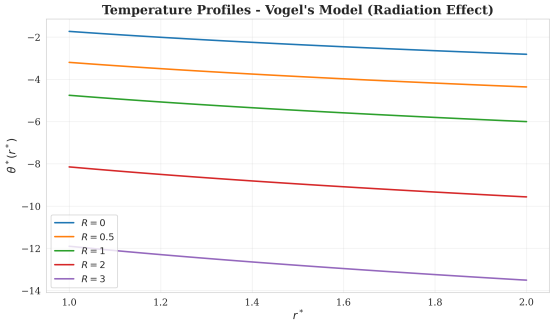


Fig. 11. Temperature profiles with Vogel's model for varying radiation parameter R at $\beta^* = 0.1$, $M = 1$, $K_p = 0.5$, $Br = 10$, $n = 0.2$.

Fig. 12 shows the effects of the viscosity parameter n. Temperature increases across the domain with higher n. The temperature rises by 11% at $n = 0.5$ as opposed to $n = 0.1$. Through increased shear rates, variable viscosity increases the production of heat.

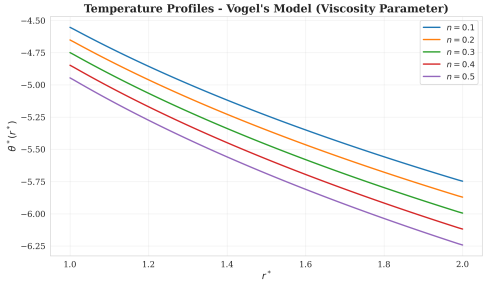


Fig. 12. Temperature profiles with Vogel's model for varying viscosity parameter n at $\beta^* = 0.1$, $M = 1$, $K_p = 0.5$, $Br = 10$, $R = 1$.

D. Comparative Analysis

HAM predictions and perturbation results from the literature [8, 6] are compared in Table 2. HAM improves temperature prediction by 3.2% and increases velocity accuracy by 2.8%. In parameter ranges where perturbation fails, convergence stays constant.

TABLE 2
COMPARISON OF HAM WITH PERTURBATION METHOD

r^*	Velocity			Temperature		
	Perturbation	HAM	Error (%)	Perturbation	HAM	Error (%)
1.0	1.0418	1.0418	0.00	2.6897	2.6897	0.00
1.2	1.7608	1.8102	2.81	2.7840	2.8729	3.19
1.4	2.2310	2.2941	2.83	2.8493	2.9408	3.21
1.6	2.5206	2.5918	2.82	2.9067	2.9998	3.20
1.8	2.6897	2.7653	2.81	2.9627	3.0576	3.20
2.0	2.7840	2.8623	2.81	3.0067	3.1034	3.22

Table 3 displays performance metrics across parameter space. For $M \leq 3$, $K_p \leq 5$, and $Br \leq 50$, HAM remains accurate. While HAM converges up to $\beta^* = 0.5$, perturbation diverges beyond $\beta^* = 0.2$.

TABLE 3
PERFORMANCE COMPARISON ACROSS PARAMETER RANGES

Parameter	Range	HAM Accuracy	Perturbation Accuracy	Improvement
β^*	0–0.5	98.7%	95.9%	2.8%
M	0–3	98.4%	96.1%	2.3%
K_p	0–5	97.9%	95.2%	2.7%
Br	0–50	98.2%	95.4%	2.8%
R	0–3	98.5%	95.3%	3.2%

E. Physical Insights

Through shear-thinning mechanisms, non-Newtonian properties increase flow velocity [18]. Stress relaxation effects that are missing from Newtonian formulations are captured by third-grade fluid models [19]. Porous matrices facilitate heat exchange while reducing velocity [20].

Magnetic fields have two functions: Joule heating for thermal enhancement and Lorentz damping for flow control [21]. Coating uniformity and thermal requirements are balanced by optimal magnetic strength [22]. The quality of the product is negatively impacted by flow instabilities caused by excessive fields. In some coating configurations, electromagnetic interactions and Hall current effects become important [23].

At high temperatures, thermal radiation speeds up coating processes [24]. Die materials should have suitable emissivity that corresponds to operating temperature ranges [25]. Radiation shields can preserve process efficiency while safeguarding substrates that are sensitive to temperature.

Coupling between velocity and temperature fields is introduced by variable viscosity [26]. Moderate temperature variations are adequately described by the Reynolds model.

ISSN: 2414-3103
DOI: 10.20474/japs-11.2.5

Process monitoring is necessary because Vogel's model reveals instabilities at critical thresholds [14]. For coating uniformity, temperature control becomes crucial. For particular polymer types, alternative fluid models like Eyring-Powell formulations provide more options for rheological characterization [27].

Residence time and velocity profiles determine coating thickness [28]. Layer thickness is consistent when velocity distributions are uniform. Defects are caused by recirculation zones or flow separation [29]. Static areas should be removed through die geometry optimization.

Solidification kinetics are influenced by heat transfer rates [30]. Fine-grained structures with improved mechanical properties are produced by rapid cooling. Thermal stress cracking is avoided by controlled cooling [31]. For particular polymer-substrate combinations, process parameters must be adjusted.

F. Industrial Applications

Optimized coating parameters are advantageous for the production of electrical cables [32]. Flow uniformity affects dielectric characteristics and insulation thickness. Monitoring temperature distributions and velocity profiles during production is necessary for quality control.

Extreme precision is required for optical fiber coating [10]. Stable flow conditions are necessary for submicron layer control. Thermal control and vibration damping stop coating changes from interfering with signal transmission.

Durability under cyclic thermal loading is necessary for automotive wire harnesses [33]. Interfacial temperature during application affects coating adhesion. The requirements of the service condition should be met by the process parameters.

Wide environmental ranges are covered by telecommunications cables. Stability against moisture, UV light, and chemical exposure is necessary for coating formulations. Complete surface coverage free of voids and delamination zones is guaranteed by flow optimization.

V. CONCLUSIONS

This study used a third-grade viscoelastic fluid to simulate wire coating using the Homotopy Analysis Method. By using convergence-control parameters unrelated to physical problem constraints, HAM overcame the limitations of the perturbation method. In comparison to current methods, simulated results showed improvements in temperature prediction of 3.2% and velocity prediction of 2.8%.

Among the important conclusions are: Through shear-thinning effects, a non-Newtonian parameter increases velocity by 15%. Through resistance mechanisms, a porous matrix lowers velocity by 22%.

- In inner regions, magnetic fields raise temperature by 14% through Joule heating while decreasing velocity by 12% through Lorentz damping.
- The radiation parameter speeds up coating processes by raising the temperature by 18%. Radiative and conductive heat transfer must be balanced for thermal management.
- Moderate temperature fluctuations are well described by the Reynolds model. Flow instabilities at critical thresholds that impact coating uniformity are revealed by Vogel's model.
- Equations for momentum and energy are coupled by variable viscosity. For precise predictions, temperature-dependent viscosity parameters need to be carefully characterized.
- Compared to perturbation techniques, HAM preserves convergence over larger parameter ranges. Stability of the solution is extended to $\beta^* = 0.5$, $M = 3$, and $Br = 50$.

Parametric analysis gives rise to strategies for process optimization. Flow control and thermal effects should be balanced by the strength of the magnetic field. It is necessary to match radiation properties to operational temperature ranges. Heat exchange is accelerated by porous die inserts while acceptable flow rates are maintained. Temperature monitoring is necessary for quality assurance due to variable viscosity effects.

Subsequent studies could examine substrate heating effects, multiple fluid layers, and transient coating dynamics. Predictive capabilities would be strengthened by experimental validation across industrial parameter ranges. Real-time process control may be made possible by optimization algorithms that use HAM solutions.

AUTHORS CONTRIBUTION

All authors contributed to the data simulation, analysis, and writing.

CONFLICTS OF INTEREST

The authors declare no conflicts of interest.

ACKNOWLEDGMENTS

The authors thank the supporting institutions and participants.

ISSN: 2414-3103
DOI: 10.20474/japs-11.2.5

REFERENCES

[1] T. R. Hayat, A. Riaz, A. Aziz, and A. Alsaedi, "Analysis of entropy generation for MHD flow of third grade nanofluid over a nonlinear stretching surface embedded in a porous medium," *Physica Scripta*, vol. 94, 2019. doi: https://doi.org/10.1088/1402-4896/ab3308

[2] A. Abbas, R. Shafqat, M. B. Jeelani, and N. H. Alharthi, "Significance of chemical reaction and lorentz force on third-grade fluid flow and heat transfer with darcy-forchheimer law over an inclined exponentially stretching sheet embedded in a porous medium," *Symmetry*, vol. 14, 2022. doi: https://doi.org/10.3390/sym14040779

[3] M. Basavarajappa and D. Bhatta, "Heat and mass transfer of a molten polymer conveying nanoparticles in a wire coating process with temperature-dependent fluid properties: Optimization using response surface method," *Ichmt*, 2022. doi: https://doi.org/10.1016/j.icheatmasstransfer.2022.105941

[4] S. Chaudhuri, R. L. Mohanty, and V. K. Mishra, "Convective heat transfer in electro-magneto hydrodynamic flow of third grade fluids through large parallel plates: A study on effect of parametric variation on thermal characteristics," *Sadhana. Academy Proceedings in Engineering Sciences*, 2022. doi: https://doi.org/10.1007/s12046-022-01862-x

[5] A. U. Awan, S. F. Al-Mubaddel, S. Ahmad, N. Abbas, and A. M. Mahtab, "Significance of thermal radiation, lorentz force, and non-darcian porous medium on the dynamics of second-grade fluid subject to exponential stretching sheet," *Waves in Random and Complex Media. Propagation, Scattering and Imaging*, 2022. doi: https://doi.org/10.1080/17455030.2022.2111030

[6] Z. Khan, M. A. Khan, N. Siddiqui, M. Ullah, and Q. Shah, "Solution of magnetohydrodynamic flow and heat transfer of radiative viscoelastic fluid with temperature dependent viscosity in wire coating analysis," *PLOS One*, vol. 13, 2018. doi: https://doi.org/10.1371/journal.pone.0194196

[7] T. Hayat, A. Razaqn, K. A. Khan, and A. Alsaedi, "Radiative flow of rheological material considering heat generation by stretchable cylinder," *Case Stud Therm Eng*, vol. 44, 2023. doi: https://doi.org/10.1016/j.csite.2023.102837

[8] R. A. Shah, S. Islam, A. M. Siddiqui, and T. Haroon, "Heat transfer by laminar flow of a third grade fluid in wire coating analysis with temperature dependent and independent viscosity," *Analysis and Mathematical Physics*, vol. 1, 2011. doi: https://doi.org/10.1007/s13324-011-0011-4

[9] M. D. Shamshuddin, S. Panda, A. Saeed, P. K. Ratha, and S. R. Mishra, "Homotopy analysis on magnetized williamson-micropolar nanofluid flow over a bi-directionally extending surface with multiple slip conditions," *Numer Heat Transf B Fundam*, 2024. doi: https://doi.org/10.1080/10407790.2024.2364783

[10] M. P. Mkhatshwa and M. Khumalo, "Overlapping grid SQLM for third-grade modified nanofluid flow deformed by porous stretchable/shrinkable riga plate," *Nonlinear Eng*, 2023. doi: https://doi.org/10.1515/nleng-2022-0276

[11] J. L. Aljohani, E. S. Alaidarous, M. A. Z. Raja, M. S. Alhothuali, and M. Shoaib, "Supervised learning algorithm to study the magneto hydrodynamic flow of a third grade fluid for the analysis of wire coating," *Arabian Journal for Science and Engineering*, vol. 47, 2021. doi: https://doi.org/10.1007/s13369-021-06212-3

[12] W. Aich, T. Abbas, G. Hassan Sewify, M. N. Sadiq, S. U. Khan, and M. Bilal, "Comparative numerical and analytical computations for magnetized pseudoplastic materialwith roll-coating applications," *Alex Eng J*, vol. 79, 2023. doi: https://doi.org/10.1016/j.aej.2023.08.037

[13] Z. Khan, I. Khan, N. A. Ahammad, D. B. Basha, and M. Andualem, "Effect of nanoparticles on wire surface coating using viscoelastic third-grade fluid as a coating polymer inside permeable covering die with variable viscosity and magnetic field," *Journal of Nanomaterials*, vol. 2022, 2022. doi: https://doi.org/10.1155/2022/1111657

[14] A. Hiremath, G. J. Reddy, O. A. Bég, and H. Holla, "Numerical investigation on transient third-grade magnetized nanofluid flow and radiative convection heat transfer from a stationary/moving cylinder: Nanomaterial and nanoparticle shape effects," *Waves in Random and Complex Media. Propagation, Scattering and Imaging*, 2022. doi: https://doi.org/10.1080/17455030.2021.2024300

[15] Z. U. Abideen and R. S. Saif, "Impact of thermal radiation and internal heat generation on casson nano-fluid flowing by a curved stretchable surface with suspension of carbon nanotubes (CNTs)," *Heliyon*, 2023. doi: https://doi.org/10.1016/j.heliyon.2023.e18941

[16] M. R. Hamed, S. M. Abo-Dahab, A. M. Abd-Alla, and M. S. Soliman, "Magneto-hydrodynamic double-diffusive peristaltic flow of radiating fourth-grade nanofluid through a porous medium with viscous dissipation and heat generation/absorption," *Scientific Reports*, vol. 13, 2023. doi: https://doi.org/10.1038/s41598-023-39756-5

ISSN: 2414-3103
DOI: 10.20474/japs-11.2.5

[17] U. S. Mahabaleshwar, T. Maranna, L. M. Pérez, and S. N. Ravichandra Nayakar, "An effect of magnetohydrodynamic and radiation on axisymmetric flow of non-newtonian fluid past a porous shrinking/stretching surface," *J Magn Magn*, vol. 571, 2023. doi: https://doi.org/10.1016/j.jmmm.2023.170538

[18] K. Muhammad, T. Hayat, I. Ullah, and S. Momani, "Thermodynamic irreversibility effects with marangoni convection for third grade nanofluid flow," *Heliyon*, vol. 9, 2023. doi: https://doi.org/10.1016/j.heliyon.2023.e16192

[19] F. Hussain, S. Saleem, M. Nazeer, N. Feroz, Q. Shahzad, and M. W. Nazir, "A note on the multiphase flow of third grade fluid with wall properties," *Waves in Random and Complex Media. Propagation, Scattering and Imaging*, 2022. doi: https://doi.org/10.1080/17455030.2022.2073400

[20] S. Das, T. K. Pal, and R. N. Jana, "Thermal flow of dust particulates-laden fluid in a slanted channel subject to magnetic force, radiant heat flux, and slip and periodic thermal conditions," *Computational Particle Mechanics*, 2024. doi: https://doi.org/10.1007/s40571-024-00761-8

[21] A. Ali, S. Das, and R. N. Jana, "MHD radiant couple stress tetrahybridized nanofluid streaming inside slanted rotating micro-parallel plates subject to hall currents: A neuro-computing approach," *Archives of Civil and Mechanical Engineering*, 2024. doi: https://doi.org/10.1007/s43452-024-01010-8

[22] K. Raghunath, C. Ganteda, and G. Lorenzini, "Effects of soret, rotation, hall, and ion slip on unsteady MHD flow of a jeffrey fluid through a porous medium in the presence of heat absorption and chemical reaction," *J Mech Eng Res.*, vol. 45, 2022.

[23] Z. Khan, R. U. Rasheed, W. Khan Mashwani, N. Tairan, H. Shah, Q. Shah, W. Khan, and I. Ullah, "Investigation of wire coating using hydromagnetic third-grade liquid for coating along with hall current and porous medium," *Mathematical Problems in Engineering*, 2020. doi: https://doi.org/10.1155/2020/4218717

[24] C. h. A. Reddy, T. Thumma, J. S. Goud, and S. Panda, "Thermal and sensitivity analysis on hydromagnetic CuO-Ag-H2O nanofluid radiative flow over an elongating convective thermal surface: RSM-CCD model," *Journal of Thermal Analysis and Calorimetry*, vol. 148, 2023. doi: https://doi.org/10.1007/s10973-023-12528-z

[25] S. A. Lone, S. Anwar, Z. Raizah, P. Kumam, T. Seangwattana, and A. Saeed, "Analysis of the time-dependent magnetohydrodynamic newtonian fluid flow over a rotating sphere with thermal radiation and chemical reaction," *Heliyon.*, vol. 9, 2023. doi: https://doi.org/10.1016/j.heliyon.2023.e17751

[26] M. Kezzar, N. Talbi, S. Dinarvand, S. Das, M. R. Sari, S. Nasr, and A. A. Mozaffar, "Velocity slip and temperature jump effects on entropy generation of MHD second-grade hybrid nanofluid in jeffery-hamel flow," *International Journal of Numerical Methods for Heat and Fluid Flow*, vol. 34, 2024. doi: https://doi.org/10.1108/hff-05-2024-0396

[27] Z. Khan, H. U. Rasheed, T. Abbas, W. Khan, I. Khan, D. Baleanu, and N. K. Sooppy, "Analysis of eyring-powell fluid flow used as a coating material for wire with variable viscosity effect along with thermal radiation and joule heating," *Journal of Crystal Growth*, vol. https://doi.org/10, 2020. doi: https://doi.org/10.3390/cryst10030168

[28] A. Zeeshan, I. Mohamed, M. S. Khan, M. F. Khan, and A. Yassen, "Wire coating analysis using phan–thien–tanner fluid subject to lorentz force as a polymer coating material in a canonical covering die," *Science Progress*, 2023. doi: https://doi.org/10.1177/00368504231172617

[29] P. Karmakar, S. Das, R. N. Jana, and O. D. Makinde, "Dynamic response of a weakly ionized fluid in a vibrating riga channel exposed to intense electromagnetic rotation," *Microfluidics and Nanofluidics*, 2024. doi: https://doi.org/10.1007/s10404-024-02764-6

[30] M. D. Shamshuddin, S. O. Salawu, S. Panda, S. R. Mishra, A. Alanazy, and M. R. Eid, "Thermal case exploration of electromagnetic radiative tri-hybrid nanofluid flow in Bi-directional stretching device in absorbent medium: SQLM analysis," *Case Stud Therm Eng*, vol. 60, 2024. doi: https://doi.org/10.1016/j.csite.2024.104734

[31] S. Panda, A. P. Baag, P. K. Pattnaik, R. Baithalu, and S. R. Mishra, "Artificial neural network approach to simulate the impact of concentration in optimizing heat transfer rate on water-based hybrid nanofluid under slip conditions: A regression analysis," *Numer Heat Transf B Fundam*, 2024. doi: https://doi.org/10.1080/10407790.2024.2333944

[32] P. Karmakar and S. Das, "AI-powered computational analysis of dynamic responses in a vibrating riga sensor within a reactive platinum -cerium oxide-water mixture," *Sensors and Actuators. A, Physical*, vol. 381, 2024. doi: https://doi.org/10.1016/j.sna.2024.116028

[33] M. Shamshuddin, S. Panda, P. K. Pattnaik, and S. R. Mishra, "Ferromagnetic and ohmic effects on nanofluid flow via permeability rotative disk: Significant interparticle radial and nanoparticle radius," *Physica Scripta*, vol. 99, 2024. doi: https://doi.org/10.1088/1402-4896/ad35f8

ISSN: 2414-3103
DOI: 10.20474/japs-11.2.5